J. Math. Biol.
DOI 10.1007/s00285-017-1141-6

Mathematical Biology

Greater accuracy and broadened applicability of phase reduction using isostable coordinates

Dan Wilson[1] · **Bard Ermentrout**[1]

Received: 20 December 2016 / Revised: 17 April 2017

Abstract The applicability of phase models is generally limited by the constraint that the dynamics of a perturbed oscillator must stay near its underlying periodic orbit. Consequently, external perturbations must be sufficiently weak so that these assumptions remain valid. Using the notion of isostables of periodic orbits to provide a simplified coordinate system from which to understand the dynamics transverse to a periodic orbit, we devise a strategy to correct for changing phase dynamics for locations away from the limit cycle. Consequently, these corrected phase dynamics allow for perturbations of larger magnitude without invalidating the underlying assumptions of the reduction. The proposed reduction strategy yields a closed set of equations and can be applied to periodic orbits embedded in arbitrarily high dimensional spaces. We illustrate the utility of this strategy in two models with biological relevance. In the first application, we find that an optimal control strategy for modifying the period of oscillation can be improved with the corrected phase reduction. In the second, the corrected phase reduced dynamics are used to understand adaptation and memory effects resulting from past perturbations.

Mathematics Subject Classification 92BXX (Mathematical Biology in General) · 37MXX (Approximation Methods of Dynamical Systems) · 41AXX (Approximations and Expansions) · 49J15 (Optimal Control Problems Involving ODEs)

✉ Dan Wilson
dan.d.wilson8@gmail.com

[1] Department of Mathematics, University of Pittsburgh, Pittsburgh, PA 15213, USA

Published online: 25 May 2017

1 Introduction

Phase reduction provides a tremendously useful tool in the study of weakly perturbed nonlinear oscillators by allowing the dynamics of a potentially complicated and high order differential equation of the form

$$\frac{\partial x}{\partial t} = F(x) + G(t), \quad x \in \mathbb{R}^N, \tag{1}$$

to be represented by the single variable system:

$$\frac{\partial \theta}{\partial t} = \omega + Z(\theta)^T G(x,t), \quad \theta \in \mathbb{S}^1. \tag{2}$$

Here, the state dynamics are represented by a phase of oscillation θ, the natural frequency of the unperturbed oscillation is given by ω, $G \in \mathbb{R}^N$ is a small perturbation, $Z(\theta) \in \mathbb{R}^N$ is the phase response curve (PRC), and ^{T} indicates the matrix transpose. Such reduction strategies have had a tremendous impact on the study of limit cycle oscillators with a wide variety of applications in recent decades (Kuramoto 1984; Winfree 2001; Hoppensteadt and Izhikevich 1997; Ermentrout and Terman 2010). An essential characteristic of oscillators that can be represented by (2) is that they remain close to the limit cycle; as the state moves farther from the limit cycle, (2) becomes a worse approximation for the phase dynamics of the system (Kuramoto 1997). Generally, this requires the magnitude of external perturbations to be small compared to the Floquet multipliers (Guckenheimer and Holmes 1983) associated with the directions transverse to the periodic orbit.

Despite these limitations, recent progress has allowed for the use of phase reduction when some of the components of the external perturbations are large but oscillating at sufficiently slow (Kurebayashi et al. 2013; Park and Ermentrout 2016), or fast (Pyragas and Novičenko 2015) frequencies when compared to the natural frequency of the limit cycle oscillator. These results represent significant progress in dealing with the fundamental weak forcing limitation, but still do not allow for larger more general perturbations to a limit cycle oscillator.

An alternative strategy for studying strongly forced limit cycle oscillators is to calculate the isochrons of a system directly (Osinga and Moehlis 2010; Detrixhe et al. 2016; Huguet and Llave 2013). Such computations can provide insight into a system under study, allowing one to understand how large perturbations affect the phase dynamics and uncovering 'phaseless sets' (Guckenheimer 1975) which have proven to be of use in control applications (Nabi et al. 2013). However, practical implementation of strategies require knowledge of the full state dynamics of the system, making them difficult to apply in higher dimensions. Another strategy for addressing the breakdown of (2) at locations away from the periodic orbit has come from the development of an augmented set of coordinates for both the asymptotic phase and the coordinates transverse to the periodic orbit (Guillamon and Huguet 2009; Castejón et al. 2013) for exponentially attracting periodic orbits. While these new coordinate systems allow for a more convenient study of a system of interest, they are also computationally challenging to to implement in high dimensional systems.

As a concrete example of the limitations of (2) in the reduction of a nonlinear system (1), consider the radial isochron clock (Strogatz 1994),

$$\begin{aligned}\frac{da}{dt} &= \sigma a - b - \sigma a(a^2 + b^2),\\ \frac{db}{dt} &= a + \sigma b - \sigma b(a^2 + b^2) + g(t),\end{aligned} \tag{3}$$

with $\sigma > 0$, and $g(t)$ representing a perturbation to the b coordinate. In radial coordinates, i.e. $\tan(\theta) = b/a$, $r^2 = a^2 + b^2$, one can verify that equation (3) becomes

$$\begin{aligned}\frac{dr}{dt} &= \sigma r(1 - r^2) + g(t)\sin(\theta).\\ \frac{d\theta}{dt} &= 1 + g(t)\cos(\theta)/r.\end{aligned} \tag{4}$$

This coordinate transformation allows us to derive the phase reduced dynamics almost immediately. By noticing that unperturbed dynamics settle to a solution with $r = 1$, the phase reduced dynamics on the limit cycle are

$$\frac{d\theta}{dt} = 1 + \cos(\theta)g(t), \tag{5}$$

Equation (5) represents a standard phase reduction of the form (2) and is valid when perturbations from the limit cycle are small. However, a phase reduction of the form (5) will not always be enough to accurately represent the dynamics of (3). For instance, as shown in Fig. 1, two initial conditions at the same phase can have significantly different responses to external perturbations when their radial coordinates differ. Indeed, from

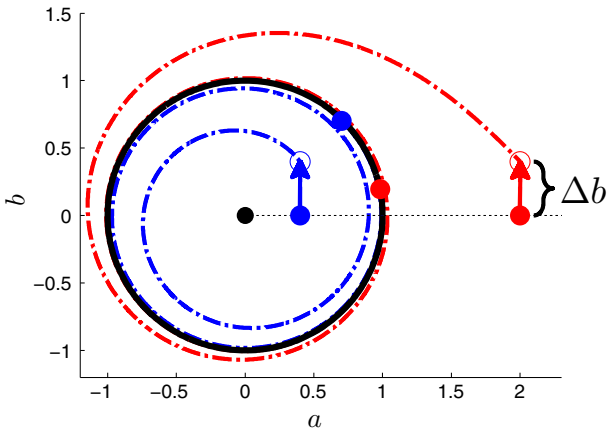

Fig. 1 Two initial conditions of (3) with $\theta = 0$ are perturbed in the b direction. *Open circles* indicate the position after perturbation and *arrows* indicate the direction of the perturbation. While the magnitude and timing of each perturbation is identical, the change in phase differs based on the initial value in the radial direction. *Colored dots* indicate the initial and final conditions of each trajectory (color figure online)

(4), the effect of a perturbation on θ is inversely proportional to r. When the nonlinear system is sufficiently far from its periodic orbit, a phase reduction of the form (2) no longer accurately characterizes effect of small perturbations on the phase dynamics.

In this work, we derive an augmented and closed form set of equations to correct for changes to the phase dynamics for locations farther from the periodic orbit. The analysis draws from the recently developed isostables coordinates for systems with periodic orbits. Intuitively, isostable coordinates give a sense of how long it will take an initial condition to approach an associated attractor. Previously, (Ichinose et al. 1998; Rabinovitch et al. 1994; Roberts 1989) investigated systems for which this attractor is a fixed point. For these systems, the notion of a transient attractor, hidden structure, or slow manifold can be used to understand the convergence of an excitable system towards its stable equilibrium. These ideas were later extended by Mauroy et al. (2013) which coined the term 'isostables' to describe level sets of initial conditions which approach the fixed point together, in a well-defined sense. In Mauroy et al. (2013), the use of isostables is limited a system's approach toward a fixed point, and Wilson and Moehlis (2016) modified this definition for use when the system approaches a limit cycle solution.

The augmented phase reduced coordinates used in this work are similar to phase-amplitude coordinates (Shirasaka et al. 2017; Wedgwood et al. 2013; Castejón et al. 2013), which have been used to understand the behavior of limit cycle oscillators in directions that are transverse to the periodic orbit. The resulting phase-amplitude coordinate transformation varies depending on the manner in which the transverse coordinate system is defined and has been useful, for example, in investigating the behavior of periodically forced oscillators (Wedgwood et al. 2013), or developing control strategies to limit the magnitude of excursions from a stable limit cycle (Shirasaka et al. 2017).

As we show in the results to follow, isostable coordinates provide a natural reduced coordinate system for understanding how perturbations will affect the phase reduced dynamics. The resulting reduction is valid for general systems of arbitrary dimension and can be applied for general perturbations allowing for a better understanding of the dynamical behavior of systems with stronger external forcing. This paper is organized as follows: Section 2 details a strategy for correcting the phase reduced dynamics when the system is not on the limit cycle. Section 3 details the relationship between isostable coordinates and perturbations to the periodic orbit in order to develop a closed set of phase reduced equations. Section 4 provides examples of this reduction strategy applied to various systems. Specifically we find that this control strategy allows for the use of larger magnitude perturbations in an optimal control problem and can also be used to understand the effects of memory in a periodic oscillator that is repeatedly perturbed by external forcing. Section 5 gives concluding remarks.

2 Calculation of the gradient and hessian of the phase on the periodic orbit

Generally, in order to approximate an equation of the form (1) by its phase reduction (2), the PRC (i.e. the gradient of the phase, $Z(\theta)$) must be calculated at all points

along the periodic orbit. Such a calculation can be performed, for instance, by finding an appropriately normalized solution to the adjoint equation (Ermentrout 2002; Govaerts and Sautois 2006). In order to determine how the gradient of the phase changes for locations that are near the periodic orbit, we will need to calculate the Hessian matrix of second partial derivatives along the periodic orbit. This section develops a computational strategy for such a calculation.

To begin, consider a stable limit cycle solution of (1) with period T. Here, $x(t) \in \mathbb{R}^N$ is the state vector, $F(x) = [f_1(x)\ f_2(x)\ \ldots\ f_N(x)]^T$ represents the natural system dynamics, and all other parameters are defined directly below (1). We will define the unperturbed flow (i.e. with $G \equiv 0$) of (1) as $\phi : \mathbb{R} \times \mathbb{R}^N \to \mathbb{R}^N$ so that $\phi(t, x_0)$ represents the solution of $\dot{x} = F(x)$ with initial condition x_0.

It is often useful to parameterize the periodic orbit, γ, of the vector yield (1) by a phase $\theta \in [0, 2\pi]$ defined so that for some arbitrary location $x_0 \in \gamma$, $\theta(x_0) = 0$, with all remaining phases defined such that $\theta(\phi(t, x_0)) = 2\pi t/T$. The notion of phase can be extended in the basin of attraction, $\mathcal{B}_\gamma$ of the limit cycle using the notion of isochrons, which are locations in phase space which share the same asymptotic convergence to the periodic orbit. Defined more rigorously, for $x_1 \in \gamma$, the $\theta(x_1)$ isochron is the set of all initial conditions $x_2 \in \mathcal{B}_\gamma$ such that

$$\lim_{t\to\infty} ||\phi(t, x_1) - \phi(t, x_2)|| = 0. \tag{6}$$

In this way, $\theta(x)$ for any $x \in \mathcal{B}_\gamma$ can be defined as the particular isochron associated with x (Winfree 2001; Osinga and Moehlis 2010). Transforming (1) to phase coordinates, from the chain rule we have

$$\begin{aligned}\dot{\theta} &= \left.\frac{\partial\theta}{\partial x}\right|_x \cdot \frac{\partial x}{\partial t},\\ &= \left.\frac{\partial\theta}{\partial x}\right|_x \cdot (F(x) + G(t)),\\ &= \omega + \left.\frac{\partial\theta}{\partial x}\right|_x G(t).\end{aligned} \tag{7}$$

In the second line, we have used the fact that the unperturbed dynamics (i.e. when G(t) = 0) satisfy (c.f. Ermentrout and Kopell 1991)

$$\dot{\theta} = \omega, \tag{8}$$

where $\omega = 2\pi/T$ so that $\left.\frac{\partial\theta}{\partial x}\right|_x \cdot F(x) = \omega$. Equation (7) represents a one dimensional reduction of (1), but is not particularly useful in its present form, as the gradient of the phase is still dependent on the state of the system. For this reason, systems are typically analyzed in the vicinity of a small neighborhood of their limit cycles, for which the PRC can be calculated using adjoint methods (Hoppensteadt and Izhikevich 1997; Brown et al. 2004; Ermentrout and Kopell 1991). Restricting attention to a close neighborhood of the limit cycle allows (7) to be written as a closed set of equations

$$\dot{\theta} = \omega + Z(\theta)^T G(t) + \mathcal{O}(x(t) - x^\gamma(\theta)). \tag{9}$$

Here, $x^\gamma(\theta)$ is defined as the intersection of the intersection of γ and the $\theta(x)$ level set, and $Z(\theta) \equiv \frac{\partial\theta}{\partial x}\big|_{x^\gamma(\theta)}$ is generally referred to as the PRC. For clarity, the dependence of θ on t has been dropped in equation (9). The utility of the reduction (9) hinges on the assumption that the state dynamics remain close to the limit cycle. For an arbitrary location $x_p = x_0 + \Delta x$, Taylor expansion of the phase field about x_0 yields

$$\nabla_{x_p}\theta = \nabla_{x_0}\theta + \nabla_{x_0}(\nabla\theta)\Delta x + \mathcal{O}(\Delta x^3). \tag{10}$$

Here, $\nabla_x\theta$ is the gradient of θ evaluated at x and $\nabla_x(\nabla\theta)$ is the Hessian matrix of second derivatives of θ, evaluated at x. For simplicity of notation, we let $H_{\theta,x} \equiv \nabla_x(\nabla\theta)$. For $x_0 = x^\gamma(\theta)$, $\nabla_{x_0}\theta$ is simply the PRC, $Z(\theta)$, for which there are well-established strategies available for its calculation (Hoppensteadt and Izhikevich 1997; Brown et al. 2004; Ermentrout and Kopell 1991). With a similar technique used in the derivation of the adjoint equation presented in Brown et al. (2004), let $x^\gamma(\theta(t)) \in \gamma$ be a solution of (1) evolving along the limit cycle. Consider a small, arbitrary perturbation Δx to that trajectory at $t = 0$. For all remaining $t > 0$, assume that $G = 0$ and let $x_\epsilon(t) = x^\gamma(\theta(t)) + \Delta x(t)$ represent this perturbed trajectory. Second order expansion of (1) yields

$$\frac{d\Delta x(t)}{dt} = J(x^\gamma(t))\Delta x(t) + \frac{1}{2}\begin{bmatrix} \Delta x^T(t) H_1(x^\gamma(t)) \\ \Delta x^T(t) H_2(x^\gamma(t)) \\ \vdots \\ \Delta x^T(t) H_N(x^\gamma(t)) \end{bmatrix} \Delta x(t) + \mathcal{O}(\Delta x^3). \tag{11}$$

Here, $J(x(t)) \equiv \nabla F(x)|_{x(t)}$ is the Jacobian matrix, and $H_i(x(t)) \equiv \nabla(\nabla f_i(x))|_{x(t)}$ is the Hessian matrix of second partial derivatives of f_i. Note that for clarity of notation we have dropped the explicit θ dependence from $x^\gamma(\theta(t))$. We can also write the phase shift due to this initial perturbation at $t = 0$ as

$$\Delta\theta = (\nabla_{x^\gamma(t)}\theta)^T \Delta x + \frac{1}{2}\Delta x^T H_{\theta,x^\gamma(t)}\Delta x + \mathcal{O}(\Delta x^3). \tag{12}$$

Using the insight given in Brown et al. (2004), after the initial perturbation at $t = 0$, $\Delta\theta$ does not change in time. Taking the time derivative of (12) yields,

$$\begin{aligned} 0 = &\left(\frac{d\nabla_{x^\gamma(t)}\theta}{dt}\right)^T \Delta x + (\nabla_{x^\gamma(t)}\theta)^T \left(\frac{d\Delta x}{dt}\right) + \frac{1}{2}\left(\frac{d\Delta x}{dt}\right)^T H_{\theta,x^\gamma(t)}\Delta x \\ &+ \frac{1}{2}\Delta x^T \left(\frac{dH_{\theta,x^\gamma(t)}}{dt}\right)\Delta x + \frac{1}{2}\Delta x^T H_{\theta,x^\gamma(t)}\left(\frac{d\Delta x}{dt}\right) + \mathcal{O}(\Delta x^3). \end{aligned} \tag{13}$$

Substituting (11) into (13) and keeping terms up to leading order Δx^2 yields

$$0 = \left(\frac{d\nabla_{x^\gamma(t)}\theta}{dt}\right)^T \Delta x + (\nabla_{x^\gamma(t)}\theta)^T \left(J(x^\gamma(t))\Delta x + \frac{1}{2}\begin{bmatrix} \Delta x^T H_1(x^\gamma(t)) \\ \Delta x^T H_2(x^\gamma(t)) \\ \vdots \\ \Delta x^T H_N(x^\gamma(t)) \end{bmatrix} \Delta x \right)$$
$$+ \frac{1}{2}\Delta x^T J^T(x^\gamma(t)) H_{\theta,x^\gamma(t)} \Delta x + \frac{1}{2}\Delta x^T \left(\frac{dH_{\theta,x^\gamma(t)}}{dt}\right)\Delta x$$
$$+ \frac{1}{2}\Delta x^T H_{\theta,x^\gamma(t)} J(x^\gamma(t))\Delta x + \mathcal{O}(\Delta x^3). \tag{14}$$

Collecting terms up to leading order Δx from (14) yields

$$0 = \left(\frac{d\nabla_{x^\gamma(t)}\theta}{dt}\right)^T \Delta x + (\nabla_{x^\gamma(t)}\theta)^T J(x^\gamma(t))\Delta x, \tag{15}$$

which, since Δx is arbitrary, can be manipulated as in Brown et al. (2004) to yield the familiar adjoint equation:

$$\frac{d\nabla_{x^\gamma(t)}\theta}{dt} = -J(x^\gamma(t))^T \nabla_{x^\gamma(t)}\theta, \tag{16}$$

whose periodic solution when normalized so that $(F(x^\gamma(t)))^T \nabla_{x^\gamma(t)}\theta = \omega$ gives the system's PRC. Now, collecting the $\mathcal{O}(\Delta x^2)$ terms from (14) yields

$$0 = (\nabla_{x^\gamma(t)}\theta)^T \begin{bmatrix} \Delta x^T H_1(x^\gamma(t)) \\ \Delta x^T H_2(x^\gamma(t)) \\ \vdots \\ \Delta x^T H_N(x^\gamma(t)) \end{bmatrix} \Delta x + \Delta x^T J^T(x^\gamma(t)) H_{\theta,x^\gamma(t)} \Delta x$$
$$+ \Delta x^T \left(\frac{dH_{\theta,x^\gamma(t)}}{dt}\right)\Delta x + \Delta x^T H_{\theta,x^\gamma(t)} J(x^\gamma(t))\Delta x. \tag{17}$$

Rewriting (17) gives

$$0 = \Delta x^T \big[Z_1(x^\gamma(t)) \cdot H_1(x^\gamma(t)) + Z_2(x^\gamma(t)) \cdot H_2(x^\gamma(t))$$
$$+ \cdots + Z_N(x^\gamma(t)) \cdot H_N(x^\gamma(t)) \big]\Delta x$$
$$+ \Delta x^T J^T(x^\gamma(t)) H_{\theta,x^\gamma(t)} \Delta x + \Delta x^T \left(\frac{dH_{\theta,x^\gamma(t)}}{dt}\right)\Delta x$$
$$+ \Delta x^T H_{\theta,x^\gamma(t)} J(x^\gamma(t))\Delta x, \tag{18}$$

where $Z_i(x(t)) \equiv \partial\theta/\partial x_i|_{x^\gamma(t)}$. Recall that the above equation holds for arbitrary perturbations, Δx so that

$$\frac{dH_{\theta,x^\gamma(t)}}{dt} = -\sum_{k=1}^{N}\left[Z_k(x^\gamma(t)) \cdot H_k(x^\gamma(t))\right] - J^T(x^\gamma(t))H_{\theta,x^\gamma(t)} - H_{\theta,x^\gamma(t)}J(x^\gamma(t)). \tag{19}$$

The differential equation (19) must be solved subject to the constraints of T-periodicity along the periodic orbit. Furthermore, if all second partial derivatives of the phase field exist and are continuous so in a neighborhood of the periodic orbit, $H_{\theta,x^\gamma(t)} \in \mathbb{R}^{N\times N}$ is symmetric. A normalizing condition is derived by starting with (16)

$$\begin{aligned} -J(x^\gamma(t))^T\nabla_{x^\gamma(t)}\theta &= \frac{d\nabla_{x^\gamma(t)}\theta}{dt}, \\ &= \frac{\partial\nabla_{x^\gamma(t)}\theta}{\partial x}\left.\frac{\partial x}{\partial t}\right|_{x^\gamma(t)}, \\ &= H_{\theta,x^\gamma(t)}F(x^\gamma(t)). \end{aligned} \tag{20}$$

Intuitively, equation (20) mandates that for an infinitesimal perturbation along the periodic orbit, the change in the PRC calculated according to the adjoint equation (16) must match the change in PRC calculated using information about $H_{\theta,x(t)}$. With knowledge of $H_{\theta,x(t)}$, the second order phase reduced dynamics become

$$\dot{\theta} = \omega + \epsilon(Z(\theta) + H_{\theta,x^\gamma(\theta)}\Delta x)^T G(t) + \mathcal{O}(\Delta x^2), \tag{21}$$

Equation (21) represents the first step towards correcting the phase dynamics for locations not on the limit cycle. In the following sections, we will illustrate how near the limit cycle, $x(t)$ can be represented as a function of isostable coordinates allowing for the dynamics to be studied in a simplified coordinate system.

3 Using isostable coordinates to find a closed set of phase reduced equations

Equation (21) provides a correction for the gradient of the phase field for locations in phase space that are not on the periodic orbit. However, this equation is still a function of Δx, which limits its practical utility. In order to characterize how $\Delta x(t)$ changes in response to perturbations, we employ Floquet theory to understand the transient dynamics of perturbations to the limit cycle. First, using methods presented in Wilson and Moehlis (2016) we define a Poincaré map using the notion of isochrons. Letting $\Gamma_0 = \{x|\theta(x) = 0\}$ define a Poincaré surface we define the following Poincaré map for (1) when $G \equiv 0$:

$$P : \Gamma_0 \to \Gamma_0;$$

$$x \to \phi(T, x). \tag{22}$$

Recall that ϕ represents the unperturbed flow of the system and T is the natural period of the limit cycle. Because the Poincaré surface is defined using isochrons, any initial condition in Γ_0 first returns to Γ_0 at time T. This map has a fixed point $P(x_{\theta_0}) = x_{\theta_0}$ for $x_{\theta_0} \in \gamma$ and on the $\theta = 0$ isochron. Close to this fixed point, one can approximate (22) with a linear mapping

$$\phi(T, x) = x_{\theta_0} + J_P(x - x_{\theta_0}) + \mathcal{O}(||x - x_{\theta_0}||^2). \tag{23}$$

Here $J_P = d\phi(T, x)/dx|_{x=x_{\theta_0}}$. We assume that J_P is diagonalizable and let $V \in \mathbb{R}^{N\times N}$ be a matrix whose columns define a basis of unit length eigenvectors v_k with associated eigenvalues λ_k for $k = 1 \ldots N$. Because the system admits a limit cycle solution, at least one eigenvalue is equal to one (since a perturbation along the periodic orbit does not decay). By convention, we will let $\lambda_N = 0$ and define isostable coordinates (c.f. Wilson and Moehlis 2016) for all $\lambda_i \neq 1$ as

$$\psi_i(x) = \lim_{j\to\infty} \left[e_i^T V^{-1}(\phi(t_\Gamma^j, x) - x_{\theta_0}) \exp(-\log(\lambda_i)t_\Gamma^j/T)\right], \tag{24}$$

t_Γ^j is the jth return time to Γ_0 under the flow and e_i is a vector with 1 in the ith position and zeros elsewhere. In the definition above, as the sequence $\{\phi(t_\Gamma^j, x)\}_{j\in\mathbb{N}}$ approaches the fixed point of the Poincaré map, its convergence can be well approximated by $(\phi(t_\Gamma^j, x) - x_{\theta_0}) = \sum_{j=1}^N \left[s_j(x)v_j\lambda^j\right]$, where s_j represent coordinates in the basis of eigenvectors of J_p. Keeping this in mind, note that $e_i^T V^{-1}$ yields a left eigenvector of J_p, which is used to select for the component of $(\phi(t_\Gamma^j, x) - x_{\theta_0})$ in the v_i direction. Furthermore, using the definition of isochrons, $t_\Gamma^{j+1} - t_\Gamma^j = T$, which implies $\exp(-\log(\lambda_i)t_\Gamma^{j+1}/T) = \frac{1}{\lambda}\exp(-\log(\lambda_i)t_\Gamma^j/T)$. Therefore, the multiplication of $e_i^T V^{-1}(\phi(t_\Gamma^j, x) - x_{\theta_0})$ by $\exp(-\log(\lambda_i)t_\Gamma^j/T)$ converges to a scalar as $j \to \infty$. The resulting scalar is the isostable coordinate.

Intuitively, larger values of ψ_i correspond to larger distances from the stable limit cycle. As we will show, the use of isostable coordinates will allow for the derivation of a closed set of equations for $\Delta x_\theta(t)$, the distance of a given trajectory from the limit cycle. The definition (24) is analogous the definition of isostables from Mauroy et al. (2013) for use when the dynamics relax to a fixed point rather than a limit cycle.

3.1 Isostable eduction for systems with periodic orbits

By noting that $dt_\Gamma^j/dt = -1$, and letting $q^j(x) \equiv e_i^T V^{-1}(\phi(t_\Gamma^j, x) - x_{\theta_0})$ $\exp(-\log(\lambda_i)t_\Gamma^j/T)$, differentiating both sides of (24) with respect to t yields

$$\frac{d\psi_i(x)}{dt} = \lim_{j\to\infty}\left[\frac{dq^j(x)}{dt_\Gamma^j}\frac{dt_\Gamma^j}{dt}\right],$$

$$\nabla_x \psi_i \cdot \frac{dx}{dt} = \frac{\log(\lambda_i)}{T} \lim_{j\to\infty} \left[q^j(x) \right],$$
$$\nabla_x \psi_i \cdot F(x) = \frac{\log(\lambda_i)}{T} \psi_i, \tag{25}$$

where $\nabla_x \psi_i$ is the gradient of ψ_i evaluated at x which we will refer to as an isostable response curve (IRC). Equation (25) indicates that in the absence of external perturbations, isostable coordinates decay exponentially with a fixed time constant, a useful feature for this and other phase-amplitude coordinate systems (c.f. Shirasaka et al. 2017; Wedgwood et al. 2013; Castejón et al. 2013).

Starting with (1) and changing to isostable coordinates, by the chain rule

$$\begin{aligned} \frac{d\psi_i(x)}{dt} &= \nabla_x \psi_i \cdot (F(x) + G(t)), \\ &= \kappa_i \psi_i(x) + \nabla_x \psi_i G(x), \end{aligned} \tag{26}$$

where in the second line we have used (25), and $\kappa_i \equiv \log(\lambda_i)/T$. Much like how the PRC can be calculated by finding solutions to the adjoint equation along the periodic orbit, a similar equation can be derived for use in calculating $\nabla_{x^\gamma(t)} \psi_i$, defined as the gradient of the isostable coordinate evaluated at the periodic orbit. To do so, following the derivation from Wilson and Moehlis (2016), consider a small perturbation Δx to the periodic orbit $x^\gamma(t)$. By linearization, $\Delta x(t)$ obeys

$$\frac{d\Delta x(t)}{dt} = J(x^\gamma(t))\Delta x(t) + \mathcal{O}(||\Delta x||^2), \tag{27}$$

recalling that $J(x^\gamma(t))$ is defined as the Jacobian of F evaluated at $x^\gamma(t)$. Furthermore, the isostable shift corresponding to the perturbation $\Delta\psi_i \equiv \psi_i(x^\gamma(t) + \Delta x(t)) - \psi_i(x^\gamma(t))$ can be found by the linear approximation

$$\Delta\psi_i = \nabla_{x^\gamma(t)} \psi_i \cdot \Delta x(t) + \mathcal{O}(||\Delta x||^2), \tag{28}$$

Assuming that $G \equiv 0$ after the initial perturbation, taking the derivative of (28) with respect to time yields

$$\begin{aligned} \langle d\nabla_{x^\gamma(t)} \psi_i / dt, \Delta x(t) \rangle + \left\langle \nabla_{x^\gamma(t)} \psi_i, d\Delta x(t)/dt \right\rangle &= \kappa_i \Delta\psi_i, \\ &= \langle \kappa_i \nabla_{x^\gamma(t)} \psi_i, \Delta x(t) \rangle, \end{aligned} \tag{29}$$

where the right hand side of the top equation is obtained using (26), the bottom equation is found by substituting (28), and $\langle \cdot, \cdot \rangle$ is the dot product. Manipulation of (29) yields

$$\begin{aligned} \langle d\nabla_{x^\gamma(t)} \psi_i / dt, \Delta x(t) \rangle &= -\left\langle \nabla_{x^\gamma(t)} \psi_i, d\Delta x(t)/dt \right\rangle + \left\langle \kappa_i \nabla_{x^\gamma(t)} \psi_i, \Delta x(t) \right\rangle \\ &= -\left\langle \nabla_{x^\gamma(t)} \psi_i, J(x^\gamma(t))\Delta x(t) \right\rangle + \left\langle \kappa_i \nabla_{x^\gamma(t)} \psi_i, \Delta x(t) \right\rangle \\ &= -\left\langle J(x^\gamma(t))^T \nabla_{x^\gamma(t)} \psi_i - \kappa_i \nabla_{x^\gamma(t)} \psi_i, \Delta x(t) \right\rangle. \end{aligned} \tag{30}$$

Because (30) is valid for any Δx, the following relation holds:

$$\frac{d\nabla_{x^\gamma(t)}\psi_i}{dt} = (\kappa_i I - J(x^\gamma(t))^T)\nabla_{x^\gamma(t)}\psi_i, \tag{31}$$

where I is the identity matrix. The isostable response curve is the solution of (31) subject to the normalizing condition $\nabla_{x_{\theta_0}}\psi_i \cdot v_i = 1$. Using (31) to calculate IRCs, (26) becomes:

$$\begin{aligned}\dot{\psi}_i &= \kappa_i\psi_i + \epsilon\mathcal{I}_i^T(\theta)G(t) + \mathcal{O}(\Delta x),\\ i &= 1,\ldots,N-1,\end{aligned} \tag{32}$$

where $\mathcal{I}_i(\theta) \equiv \nabla_{x^\gamma(\theta)}\psi_i$. Equation (32), much like the phase reduction (9) is accurate to leading order Δx.

3.2 Writing Δx in terms of isostable coordinates

We will now show that near the periodic orbit, Δx can be written as a function of the isostable coordinates. As in the previous section, letting $x_\epsilon(t) = x^\gamma(\theta(t)) + \Delta x(t)$ represent a solution of (1), the perturbed dynamics with $G = 0$ satisfy to leading order,

$$\frac{d\Delta x}{dt} = J(x(t))\Delta x(t) + \mathcal{O}(\Delta x^2), \tag{33}$$

where $J(x(t))$ is the Jacobian matrix evaluated at $x(t)$. Floquet theory (Grimshaw 1993; Klausmeier 2008) allows us to write solutions of (33) as

$$\Delta x(t) = \left[q_1(t)\ q_2(t)\ \ldots\ q_N(t)\right]\left[c_1\exp(\kappa_1 t)\ c_2\exp(\kappa_2 t)\ \ldots\ c_N\exp(\kappa_N t)\right]^T. \tag{34}$$

Here, the constants c_i are chosen to satisfy the initial conditions, $q_i(t) \in \mathbb{R}^N$ are T-periodic functions, and $\kappa_i = \log(\lambda_i)/T$ are referred to as as Floquet exponents. In (34), higher order terms have been dropped for notational convenience. In (33) because phase increases at a constant rate, i.e. $\dot{\theta} = \omega$, (34) can be rewritten as

$$\begin{aligned}\Delta x(t) = &\left[p_1(\theta(t))\ p_2(\theta(t))\ \ldots\ p_N(\theta(t))\right]\\ &\times\left[c_1\exp(\kappa_1 t)\ c_2\exp(\kappa_2 t)\ \ldots\ c_N\exp(\kappa_N t)\right]^T,\end{aligned} \tag{35}$$

where $p_i(\theta(0) + \omega t) = q_i(t)$. Recall from equation (24) that t_Γ^j is defined as the j^{th} return time to Γ_0 under the flow. Also, note that $\Delta x(t_\Gamma^j) = \phi(t_\Gamma^j, x_\epsilon(0)) - x_{\theta_o}$, and $\theta = 0$ by definition when the trajectory crosses the Γ_0 Poincaré section. We can use this information along with (35) to directly evaluate (24) to calculate isostable coordinates:

$$\begin{aligned}\psi_i(x) &= \lim_{j\to\infty}\Big[e_i^T V^{-1}\left(\left[p_1(0)\ \ldots\ p_N(0)\right]\left[c_1\exp(\kappa_1 t_\Gamma^i)\ \ldots\ c_N\exp(\kappa_N t_\Gamma^i)\right]^T\right)\\ &\quad\times\exp(-\log(\lambda_i)t_\Gamma^j/T)\Big],\\ &= \lim_{j\to\infty}\Big[e_i^T V^{-1}\left(\left[p_1(0)\ \ldots\ p_N(0)\right]\left[c_1\exp((\kappa_1-\kappa_i)t_\Gamma^i)\ \ldots\ c_N\exp((\kappa_N-\kappa_i)t_\Gamma^i)\right]\right).\end{aligned} \tag{36}$$

In the second line, we have used the fact that $\kappa_i = \log(\lambda_i)/T$. From the linearizion of the Poincaré map near x_{θ_o}, one can show that $p_i(\theta)$ from (35) approximately satisfies

$$\epsilon p_i(\theta) = \left[\phi(\theta(\tau)/\omega, \epsilon v_i + x_{\theta_o})\exp(-\kappa_i\tau)\right] - \phi(\theta(\tau)/\omega, x_{\theta_o}) \tag{37}$$

for $0 < \epsilon \ll 1$ allowing for relatively straightforward numerical approximation. Using (37), $p_i(0) = v_i$, and substituting this into (36) yields

$$\begin{aligned}\psi_i(x) &= \lim_{j\to\infty}\left[e_i^T V^{-1}\left[v_1\ v_2\ \ldots\ v_N\right]\left[c_1\exp((\kappa_1-\kappa_i)t_\Gamma^i)\ \ldots\ c_N\exp((\kappa_N-\kappa_i)t_\Gamma^i)\right]^T\right],\\ &= \lim_{j\to\infty}\left[e_i^T\left[c_1\exp((\kappa_1-\kappa_i)t_\Gamma^i)\ \ldots\ c_N\exp((\kappa_N-\kappa_i)t_\Gamma^i)\right]^T\right], \quad = c_i.\end{aligned} \tag{38}$$

Equation (38) states that for the choice of $p_i(t)$ in (37), the constants c_i from (34) are identical to the isostable values ψ_i. Using this result, to leading order in Δx,

$$\Delta x(t) = \sum_{i=1}^{N-1} p_i(\theta(t))\psi_i(t), \tag{39}$$

Finally, (21) and (32) from the previous sections can be used together with (39) to yield

$$\begin{aligned}\dot\theta &= \omega + \left[Z(\theta) + H_{\theta,x^\gamma(\theta)}\left(\sum_{j=1}^{N-1} p_j(\theta)\psi_j\right)\right]^T G(t) + \mathcal{O}(\Delta x)^2,\\ \dot\psi_i &= \kappa_i\psi_i + \mathcal{I}_i^T(\theta)G(t) + \mathcal{O}(\Delta x),\\ i &= 1,\ldots,N-1.\end{aligned} \tag{40}$$

While equation (40) has the same number of variables as the original equations (1), in practice, if some directions rapidly decay, i.e. if some κ_i are very negative, they can be effectively ignored. Notice that the phase dynamics truncate terms of order Δx^2 while the isostable dynamics truncate terms of order Δx. In the following section, we will derive a correction for the isostable dynamics so that both reduced coordinate systems are accurate to the same order in Δx.

3.3 A correction for the isostable response curve

We can also correct for a changing isostable response curve at locations not on the periodic orbit. In this case again letting $x_p = x_0 + \Delta x$,

$$\nabla_{x_p}\psi_i = \nabla_{x_0}\psi_i + \nabla_{x_0}(\nabla\psi_i)\Delta x + \mathcal{O}(\Delta x^3). \tag{41}$$

Here, $\nabla_x(\nabla\psi)$ is the Hessian matrix of second derivatives of ψ_i, evaluated at x. We will use the notation $H_{\psi_i,x(t)} \equiv \nabla_x(\nabla\psi_i)$. In a similar strategy to the one used for phase coordinates, we will investigate the dynamics of a small perturbation Δx to the trajectory $x(t) \in \gamma$. Assuming the perturbation is given at $t = 0$ with $G = 0$ thereafter, again letting $x_\epsilon(t) = x^\gamma(\theta(t)) + \Delta x(t)$, as previously mentioned, (11) describes the perturbed dynamics. Furthermore, the isostable shift due to this initial perturbation is

$$\Delta\psi_i = (\nabla_{x^\gamma(t)}\psi_i)^T\Delta x + \frac{1}{2}\Delta x^T H_{\psi_i,x^\gamma(t)}\Delta x + \mathcal{O}(\Delta x^3), \tag{42}$$

After this initial perturbation, $d\Delta\psi_i/dt = \kappa_i\Delta\psi_i$ [as can be seen using (25)]. Thus, differentiating both sides of (42) with respect to time yields

$$\begin{aligned}\kappa_i\Delta\psi_i = &\left(\frac{d\nabla_{x^\gamma(t)}\psi_i}{dt}\right)^T\Delta x\\ &+ (\nabla_{x^\gamma(t)}\psi_i)^T\left(J(x^\gamma(t))\Delta x(t) + \frac{1}{2}\begin{bmatrix}\Delta x^T(t)H_1(x^\gamma(t))\\ \Delta x^T(t)H_2(x^\gamma(t))\\ \vdots\\ \Delta x^T(t)H_N(x^\gamma(t))\end{bmatrix}\Delta x(t)\right)\\ &+ \frac{1}{2}\Delta x^T J^T(x^\gamma(t))H_{\psi_i,x^\gamma(t)}\Delta x + \frac{1}{2}\Delta x^T\left(\frac{dH_{\psi_i,x^\gamma(t)}}{dt}\right)\Delta x\\ &+ \frac{1}{2}\Delta x^T H_{\psi_i,x^\gamma(t)}J(x^\gamma(t))\Delta x + \mathcal{O}(\Delta x^3).\end{aligned} \tag{43}$$

Note the similarity between (43) and (14) which was derived for the phase variable. By collecting $\mathcal{O}(\Delta x)$, as shown in Wilson and Moehlis (2016), one arrives at (31). In the same sequence of steps to those which yield (17), (18), and (19) from (14), we collect all $\mathcal{O}(\Delta x^2)$ terms and manipulate to yield

$$\begin{aligned}\frac{dH_{\psi_i,x^\gamma(t)}}{dt} = &-\sum_{k=1}^{N}\left[\mathcal{I}_i^k(x^\gamma(t))\cdot H_k(x^\gamma(t))\right]\\ &- J^T(x(t))H_{\psi_i,x(t)} - H_{\psi_i,x(t)}J(x(t)) + \kappa_i H_{\psi_i,x(t)},\end{aligned} \tag{44}$$

where $\mathcal{I}_i^j(x(t)) \equiv \partial\psi_i/\partial x_j\big|_{x(t)}$. Here, the solution of (44) is subject to both periodic boundary conditions and a normalization condition

$$\begin{aligned}\kappa_i I - J(x^\gamma(t))^T\nabla_{x^\gamma(t)}\psi_i &= \frac{d\nabla_{x^\gamma(t)}\psi_i}{dt},\\ &= \frac{d\nabla_{x^\gamma(t)}\psi_i}{dx}\left.\frac{dx}{dt}\right|_{x^\gamma(t)},\\ &= H_{\psi_i,x^\gamma(t)}F(x^\gamma(t)),\end{aligned} \tag{45}$$

which is derived starting with (31). Intuitively, equation (45) mandates that for small perturbations in the direction of the periodic orbit, the change in the IRC calculated with (31) is identical to what would be found using $H_{\psi_i,x(t)}$.

After calculating $H_{\psi_i,x(t)}$, the isostable dynamics are

$$\begin{aligned}\dot{\psi}_i &= \kappa_i\psi_i + (\mathcal{I}_i(\theta) + H_{\psi_i,x^\gamma(\theta)}\Delta x)^T G(t) + \mathcal{O}(\Delta x^2),\\ &= \kappa_i\psi_i + \left[\mathcal{I}_i(\theta) + H_{\psi_i,x^\gamma(\theta)}\left(\sum_{i=j}^{N-1} p_j(\theta)\psi_j(t)\right)\right]^T G(t) + \mathcal{O}(\Delta x^2),\end{aligned} \tag{46}$$

for $i = 1 \ldots N-1$. The second line of the above equation is obtained substituting the expression for Δx from (39). Finally, adjusting for changes in the gradient of the isostable field, the isostable and phase dynamics can be written as

$$\begin{aligned}\dot{\theta} &= \omega + \epsilon\left[Z(\theta) + \sum_{j=1}^{N-1} C_j(\theta)\psi_j\right]^T G(t) + \mathcal{O}(\Delta x^2),\\ \dot{\psi}_i &= \kappa_i\psi_i + \epsilon\left[\mathcal{I}_i(\theta) + \sum_{j=1}^{N-1} D_i^j(\theta)\psi_j\right]^T G(t) + \mathcal{O}(\Delta x^2),\\ i &= 1 \ldots N-1,\end{aligned} \tag{47}$$

where

$$\begin{aligned}C_j(\theta) &\equiv H_{\theta,x^\gamma(\theta)}p_j(\theta),\\ D_i^j(\theta) &\equiv H_{\psi_i,x^\gamma(\theta)}p_j(\theta).\end{aligned} \tag{48}$$

3.4 Summarizing the steps to determine the reduced equations

In the sections to follow, we will illustrate the utility of using this reduction in the analysis of various limit cycle oscillators. For a system which displays limit cycle oscillations, the general procedure for reducing the dynamics to (47) involves the following steps:

1. Identify the periodic orbit, x^γ and use the adjoint equation (16) to calculate the PRC (this information would allow for the standard phase reduction (9).
2. The hyperplane orthogonal to the PRC at $\theta = 0$ provides a linear approximation to the Γ_0 Poincaré surface (the $\theta = 0$ isochron). Linearize the resulting Poincaré map about its fixed point. The non-unity eigenvalues and associated eigenvectors of the linearization are used to define isostable coordinates as in (24).
3. For all isostable coordinates ψ_i for which λ_i is not near zero, calculate the IRC according to (31). Isostable coordinates ψ_i for which λ_i is close to zero can usually be ignored because they decay quickly.

4. Calculate the Hessian matrices $H_{\theta,x^\gamma(\theta)}$ and $H_{\psi_i,x^\gamma(\theta)}$ for all isostable coordinates which are included in the reduction according to Eqs. (19) and (44).
5. Numerically calculate all functions p_i according to (37) associated with all isostable coordinates which are included in the reduction.
6. The information from steps 1–5 is used to calculate the reduced equation (47).

4 Examples

In the sections to follow, we will investigate the use of the reduction strategy proposed in this work in three limit cycle oscillators. The first application is relatively simple so that the gradient and Hessian of the phase and isostable coordinates can be calculated analytically. Subsequent examples will highlight biological applications for which numerical computation of all required functions using the strategies detailed in the previous sections are necessary.

4.1 Step-by-step reduction of the radial isochron clock

Here, we apply the reduction strategy to the radial isochron clock (3) and explicitly walk through the steps required as listed in Sect. 3.4. While reduction in this example can be found analytically, we note in each step how it could also be approximated numerically.

Step 1: As shown in the introductory section, in the absence of external perturbations, this system (3) settles to a periodic orbit $x^\gamma(\theta)$ that traces out a circle of radius 1 and moves in the counterclockwise direction. The PRC is the appropriately normalized periodic solution to the adjoint equation (16). Additionally, in this example using $\tan(\theta) \equiv b/a$, one can derive the PRC directly:

$$Z(\theta) = \nabla_{x^\gamma(\theta)}\theta = \begin{bmatrix} -\sin(\theta) \\ \cos(\theta) \end{bmatrix}. \tag{49}$$

Step 2: At $\theta = 0$, the vector $[1\ 0]$ is orthogonal to the PRC. Therefore, near the periodic orbit at $\theta = 0$, the x-axis gives a linear approximation to the Γ_0 Poincaré surface. The fixed point of the resulting Poincaré map, $P(x_{\theta_0}) = x_{\theta_0}$ is satisfied by $x_{\theta_0} = [1\ 0]^T$. Using the transformation to radial coordinates from (4), we know the dynamics of the r direction are independent of θ in the absence of external perturbation, therefore, the linearization of the Poincaré map near the fixed point is

$$P\left(x - x_{\theta_0}\right) = \begin{bmatrix} \lambda_1 & 0 \\ 0 & 1 \end{bmatrix}\left(x - x_{\theta_0}\right) + \mathcal{O}\left(\left(x - x_{\theta_0}\right)^2\right). \tag{50}$$

Furthermore, the dynamics of the radial coordinate have the analytical solution

$$r(t) = \frac{\exp \sigma t}{\sqrt{\exp 2\sigma t + 1/r^2(0) - 1}}. \tag{51}$$

One can verify analytically that as time approaches infinity,

$$r(t) - 1 = \frac{1}{2}\left[1 - \frac{1}{r(0)^2}\right]\exp(-2\sigma t). \tag{52}$$

Using (52) we find that over the course of one revolution, $r(t+T) - 1 = \exp(-4\pi\sigma)(r(t) - 1)$ so that $\lambda_1 = \exp(-4\pi\sigma)$ and that $\kappa_1 = \log(\lambda_1)/T = -2\sigma$ (recall that the return time $T = 2\pi$ time units). From (52), and the definition of isostables from (24), one can show that

$$\begin{aligned}\psi_1(r) &= \lim_{j\to\infty}\left[e_1^T V^{-1}(\phi(t_\Gamma^j, x) - x_{\theta_0})\exp(-\log(\lambda_1)t_\Gamma^j/T)\right],\\ &= [1\ 0]\begin{bmatrix}\frac{1}{2}\left(1 - \frac{1}{r^2(0)}\right)\exp(-\sigma t_\Gamma^j)\\ 0\end{bmatrix}\exp(\sigma t_\Gamma^j),\\ &= \frac{1}{2}\left[1 - \frac{1}{r^2(0)}\right].\end{aligned} \tag{53}$$

In the second line, we use the fact that V is the identity matrix and that $r = a$ when the system crosses the Poincaré section. Numerically, we could instead find λ_1 as the non-unity Floquet multiplier of linearization about the periodic orbit with V being a matrix of corresponding eigenvectors.

Step 3: In this example, we have a single isostable coordinate which represents perturbations in the radial direction. The IRC can be calculated numerically as the appropriately normalized periodic solution to (31). For this example, by noting that $\frac{\partial\psi_1}{\partial a} = \frac{\partial\psi_1}{\partial r}\frac{\partial r}{\partial a}$ and $\frac{\partial\psi_1}{\partial b} = \frac{\partial\psi_1}{\partial r}\frac{\partial r}{\partial b}$, we can also analytically derive

$$\mathcal{I}_1(\theta) = \nabla_{x^\gamma(\theta)}\psi_1 = \begin{bmatrix}\cos(\theta)\\ \sin(\theta)\end{bmatrix}. \tag{54}$$

Step 4: In order to determine how perturbations affect the system when it is perturbed from the limit cycle, Hessians of the phase and isostable coordinates must be calculated. This computation can be performed numerically, where $H_{\theta,x^\gamma(\theta)}$ and $H_{\psi_i,x^\gamma(\theta)}$ are appropriately normalized periodic solutions of (19) and (44), respectively. Notice that Eqs. (19) and (44) require knowledge of the PRC and IRCs, respectively. One can verify the following relation through direct differentiation of the PRC and IRC from steps 1 and 3:

$$\begin{aligned}H_{\theta,x^\gamma(\theta)} &= \begin{bmatrix}\sin(2\theta) & \sin^2(\theta) - \cos^2(\theta)\\ \sin^2(\theta) - \cos^2(\theta) & -\sin(2\theta)\end{bmatrix}\\ H_{\psi_1,x^\gamma(\theta)} &= \begin{bmatrix}-3\cos^2(\theta) + \sin^2(\theta) & -2\sin(2\theta)\\ -2\sin(2\theta) & -3\sin^2(\theta) + \cos^2(\theta)\end{bmatrix}.\end{aligned} \tag{55}$$

Step 5: The function p_1 relates the isostable coordinate to its location in the original a-b coordinate system. Using the definition given in (37),

$$\begin{aligned} p_1(\theta) &= \frac{1}{\epsilon}\left[\phi(\theta(\tau)/\omega, \epsilon v_i + x_{\theta_o})\exp(-\kappa_1\tau)\right] - \phi(\theta(\tau)/\omega, x_{\theta_o}), \\ &= \frac{1}{\epsilon}\left[\phi(\theta(\tau)/\omega, [(1+\epsilon)\ 0]^T)\exp(-\kappa_1\tau)\right] - \phi(\theta(\tau)/\omega, [1\ 0]^T), \\ &= \frac{1}{\epsilon}\left(\exp 2\sigma\tau \begin{bmatrix}(1+\epsilon)\exp(-2\sigma\tau)\cos(\theta)\\ (1+\epsilon)\exp(-2\sigma\tau)\sin(\theta)\end{bmatrix} - \begin{bmatrix}\cos(\theta)\\ \sin(\theta)\end{bmatrix}\right), \\ &= \begin{bmatrix}\cos(\theta)\\ \sin(\theta)\end{bmatrix}. \end{aligned} \tag{56}$$

In the third line, we use $r(t) - 1 = (r(0) - 1)\exp(-2\sigma t)$ for $r(0)$ close to 1. While equation (56) gives an exact solution for $p_1(\theta)$, analytical solutions may not always be possible. If instead the system (3) was not analytically tractable, a numerical approximation $p_1(\theta)$ could be obtained instead by first letting $x_1 = x^\gamma(0) + [\epsilon\ 0]^T = [(1+\epsilon)\ 0]^T$. Note here that x_1 is on the $\theta = 0$ isochron and that $\psi_1(x_1) = \epsilon$. The value $p_1(\theta)$ can then be approximated according to (37) as,

$$p_1(\theta) = \frac{\exp(-\kappa_1 t)\left[\phi(\theta(t)/\omega, x_1) - x^\gamma(\theta)\right]}{\epsilon}, \tag{57}$$

which can be computed numerically.

Step 6: The full equation (3) can be rewritten in phase and isostable coordinates as

$$\begin{aligned} \dot{\theta} &= \omega + \left[Z^b(\theta) + \psi_1 C_1^b(\theta)\right] g(t) \\ &= \omega + [\cos(\theta) - \psi_1\cos(\theta)]g(t), \\ \dot{\psi}_1 &= \kappa_1\psi_1 + \left[\mathcal{I}_1^b(\theta) + \psi_1 D_1^{1,b}(\theta)\right] g(t) \\ &= \kappa_1\psi_1 + [\sin(\theta) - 3\psi_1\sin(\theta)]\, g(t). \end{aligned} \tag{58}$$

with the convention $X(\theta) = [X^a(\theta)\ X^b(\theta)]^T$ for $X = Z, C_1, \mathcal{I}_1, D_1^1$.

Figure 2 gives a visual representation of the reduced system (58). The left panel shows the limit cycle as a thick black line, and isostable coordinates $\psi = -1.5$, and 0.25 are represented as dot-dashed lines. An arbitrarily chosen trajectory $x(t)$ is shown as a dashed blue line. The top-right and bottom-right panels give the gradient of the phase and isostable coordinates, respectively, evaluated at $x(t)$. Here, exact values are calculated directly from the phase and isostable coordinates. The first order approximation is shown as dot-dashed blue line and is taken from the gradient of the phase and isostable coordinates along the periodic orbit, as is the case for the standard phase reduction. The second order approximation inferred from (58). For values farther from the periodic orbit, the first order approximation suffers dramatically, and the second order approximation provides a significantly better representation of the reduced dynamics.

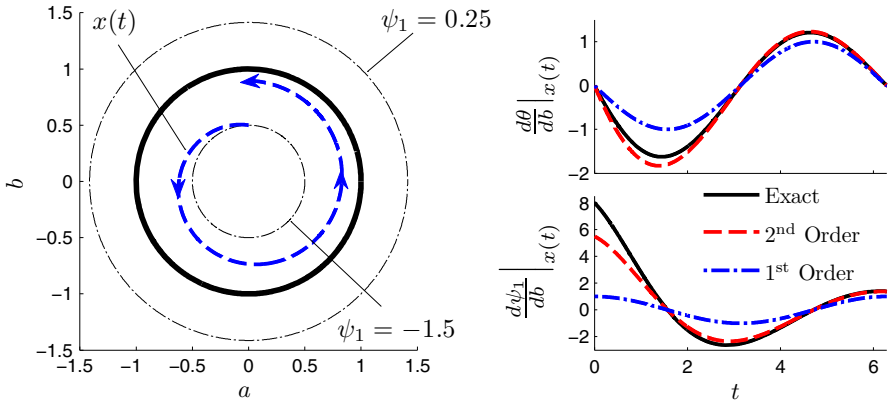

Fig. 2 The *left panel* shows level sets of two different isostable values for the system (3). An example trajectory, $x(t)$ is shown with a *dashed blue line*. The *top-right* (resp. *bottom-right panel*) gives $d\theta/db$ (resp. $d\psi_1/db$) evaluated at $x(t)$. The exact values are calculated directly from the gradient of the isostable and phase coordinates. The second order approximation is obtained from (58), for example, $d\theta/db \approx Z^b(\theta) + \psi_1 C_1^b(\theta)$. The first order approximation is obtained from the gradient evaluated at the periodic orbit, for example, $d\theta/db \approx Z^b(\theta)$ (color figure online)

4.2 Control of a model for circadian oscillations

In this section, the reduction strategy is illustrated in a model for gene regulation (Gonze et al. 2005) which has been used to model for oscillators within the suprachiasmatic nucleus which give rise to circadian oscillations:

$$\begin{aligned}
\dot{X} &= v_1 K_1^n/(K_1^n + W^n) - v_2 X/(K_2 + X) + u(t),\\
\dot{Y} &= k_3 X - v_4 Y/(K_4 + Y),\\
\dot{W} &= k_5 Y - v_6 W/(k_6 + W).
\end{aligned} \tag{59}$$

In this model, X denotes the mRNA concentration of the circadian clock gene *per* or *cry*, Y represents the associated PER or CRY protein concentration, and W gives the concentration of the active protein or its nuclear form. In this model, $u(t)$ represents an external light perturbation. We use the nominal parameter set from Figure 1 of Gonze et al. (2005). In the absence of external perturbation, the model settles to a limit cycle solution with natural period $T = 23.54$ hours.

In this example, we choose $\theta = 0$ to correspond to the moment when X reaches its maximum value on the periodic orbit. A Poincaré return map is defined using the $\theta = 0$ isochron as the Poincaré surface, and the non-identity eigenvalues of the linear approximation are numerically determined to be $\lambda_1 = 0.951$ and $\lambda_2 = 6.14 \times 10^{-6}$. In the phase and isostable coordinate transformation to follow, we will neglect the ψ_2 isostable coordinate associated with λ_2; any perturbations in this direction rapidly decay, and will assume it is approximately zero. Based on the values of the parameters T and λ_1, $\omega = 0.267$ and $\kappa_1 = -0.0021$. The right panel of Fig. 3 shows the periodic orbit, x^γ, as a thick black line. The thin black lines show orbits representing

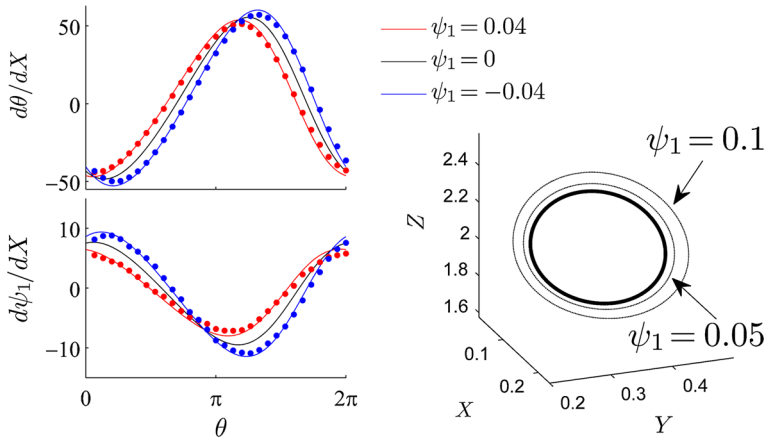

Fig. 3 The *left panels* show how the gradient of the phase and isostable coordinate changes as a function of both phase and isostable. *Dots* give numerical approximations using the direct method. *Solid lines* are calculated according to the reduction (60). Here, $\psi_1 = 0$ corresponds to a location on the limit cycle. The *right panel* shows the limit cycle solution x^γ as a *black line*. The trajectory extends outward for larger isostable values

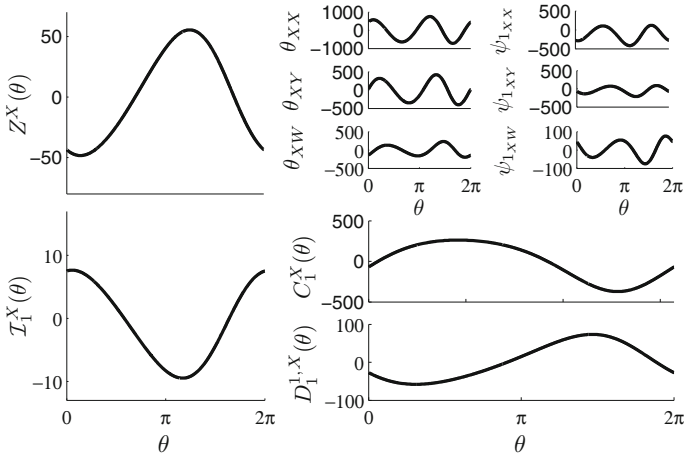

Fig. 4 Relevant parameters in the reduction of (60). The *left panels* show $Z^X(\theta)$ and $\mathcal{I}_1^X(\theta)$, which represent the effect of perturbations in the X direction on the phase and isostables when the oscillator is on the limit cycle. Near, but not on the limit cycle, $C_1^X(\theta)$ and $D_1^{1,X}(\theta)$ provide corrections based on the isostable value. These corrections are obtained by calculating the second order partial derivatives of the phase and isostable coordinates, according to equations (19) and (44), and shown in the *top-right panels*

$x^\gamma(\theta) + \psi_1 p_1(\theta)$; initial conditions along these isostable values will spiral in towards the periodic orbit in the absence of external perturbations.

The circadian system (59) is more complicated than the radial isochron clock from the previous section, and the gradient and the Hessian of the phase and isostable coordinates must be calculated numerically at locations along the periodic orbit. Fig. (4) gives the results of these calculations. Because we only have the ability to perturb

in the X direction, $Z^X(\theta)$ and $\mathcal{I}_1(\theta)$ are shown in the left panels of Fig. 4, where $Z(\theta) = [Z^X(\theta)\ Z^Y(\theta)\ Z^W(\theta)]^T$ and $\mathcal{I}_1(\theta) = [\mathcal{I}_1^X(\theta)\ \mathcal{I}_1^Y(\theta)\ \mathcal{I}_1^W(\theta)]^T$. Matrices of second derivatives $H_{\theta,x^\gamma(\theta)}$ and $H_{\psi_1,x^\gamma(\theta)}$ are calculated by finding the appropriately normalized periodic solution to (19) and (44), respectively. Only the second partial derivatives with some component in the X direction are of interest in this reduction, and these are shown in the top-right panels of Fig. 4. Here, we use the notation $\theta_{ab} \equiv \frac{d^2\theta}{(da)(db)}$. These partial derivatives are used to calculate $C_1(\theta)$ and $D_1^1(\theta)$ as defined in (48) and are shown in the bottom-right panels. The system (59) can then be rewritten in the form of (47) as:

$$\begin{aligned}\dot{\theta} &= \omega + \left[Z^X(\theta) + \psi_1 C_1^X(\theta)\right] u(t),\\ \dot{\psi}_1 &= \kappa_1\psi_1 + \left[\mathcal{I}_1^X(\theta) + \psi_1 D_1^{1,X}(\theta)\right] u(t),\end{aligned} \tag{60}$$

where $C_1^X(\theta) = e_1^T H_{\theta,x^\gamma(\theta)} p_1(\theta)$, $D_1^{1,X}(\theta) = e_1^T H_{\psi_1,x^\gamma(\theta)} p_1(\theta)$, and $e_1 = [1\ 0\ 0]^T$.

To implement the standard phase reduction as in (2) it would only be necessary to calculate and use $Z(\theta)$. However, following the strategy from Sect. 3.4 to implement a second order reduction, (60) takes into account how the gradient of phase and isostable coordinates change with varying values of ψ_1. Near the periodic orbit (i.e. for small values of ψ_1), $d\theta/dX$ and $d\psi_1/dX$ are well approximated by $Z^X(\theta) + \psi_1 C_1^X(\theta)$ and $\mathcal{I}_1^X(\theta) + \psi_1 D_1^{1,X}(\theta)$, respectively. In the left panel of Fig. 3, $d\theta/dX$ is calculated according to the reduction (60) at different values of ψ_1 and θ. These values are compared to discrete measurements with the direct method (Izhikevich 2007; Netoff and Schwemmer 2012), whereby a small perturbation ΔX is applied to the oscillator, the resulting phase (resp. isostable) change is measured as $\Delta\theta$ (resp. $\Delta\psi_1$), and the gradient of the phase (resp. isostable) coordinate is approximated by $\Delta\theta/\Delta X$ (resp. $\Delta\psi_1/\Delta X$). Overall we see good agreement between predictions and numerical observations.

Because the gradient of the phase and isostable fields can change significantly even for small isostable values, we would expect that control of the system (59) would be more accurate using (60) when compared to a strategy which does not correct for these changes, akin to the reduction used in Wilson and Moehlis (2016) where $C_1^X(\theta)$ and $D_1^{1,X}(\theta)$ are not taken into account. To illustrate this, we choose a control objective of optimally speeding up or slowing down the period of the circadian system, which is relevant to the problem of mitigating the symptoms of jet-lag (Bagheri et al. 2008; Serkh and Forger 2014; Dean et al. 2009), and may also be of relevance in treating patients with advanced or delayed sleep phase syndrome (Crowley et al. 2007; Xu et al. 2005; Wilson and Moehlis 2014). Here, we will consider all stimuli $u(t)$ which evolve $\theta(0) = 0$, $\psi_1(0) = 0$ to the final condition $\theta(T_{\text{goal}}) = 2\pi$, $\psi_1(T_{\text{goal}}) = 0$ at some prespecified time T_{goal}. In order to find the stimulus which minimizes the control effort, defined as $\int_0^{T_{\text{goal}}} u^2(t)dt$, we define a cost functional

$$\mathcal{C}_A[\dot{\Phi}, \Phi, u(t)] = u^2(t) + \xi_1\{\dot{\theta} - \omega - \left[Z^X(\theta) + \psi_1 C_1^X(\theta)\right] u(t)\}$$

$$+\xi_2\{\dot{\psi}_1-\kappa_1\psi_1-\left[\mathcal{I}_1^X(\theta)+\psi_1 D_1^{1,X}(\theta)\right]u(t)\}. \tag{61}$$

In the above cost functional, ξ_1 and ξ_2 are Lagrange multipliers which force the dynamics to satisfy the reduction (60) and $\Phi(t)=[\theta(t),\psi_1(t),\xi_1(t),\xi_2(t)]$. We also define a second cost functional

$$\mathcal{C}_B[\dot{\Phi},\Phi,u(t)]=u^2(t)+\xi_1\{\dot{\theta}-\omega-Z(\theta)u(t)\}+\xi_2\{\dot{\psi}_1-\kappa_1\psi_1+\mathcal{I}_1(\theta)u(t)\}. \tag{62}$$

which differs from (61) in that it ignores the corrections $C_1^X(\theta)$ and $D_1^{1,X}(\theta)$. The reduced equations whereby $C_1^X(\theta)$ and $D_1^{1,X}(\theta)$ are neglected as in (62) are similar to those obtained in Wilson and Moehlis (2016). For each cost functional, the Euler-Lagrange equations used to solve this calculus of variations problem are Kirk (1998)

$$\frac{\partial\mathcal{C}_k}{\partial u}=\frac{d}{dt}\left(\frac{\partial\mathcal{C}_k}{\partial\dot{u}}\right);\ \frac{\partial\mathcal{C}_k}{\partial\Phi}=\frac{d}{dt}\left(\frac{\partial\mathcal{C}_k}{\partial\dot{\Phi}}\right), \tag{63}$$

with $k=A,B$. For both cost functions, optimal solutions satisfy (63) with boundary conditions $\theta(0)=0,\theta(T_{\text{goal}})=2\pi,\psi_1(0)=0$ and $\psi_1(T_{\text{goal}})=0$. In order to satisfy this two-point boundary value problem, the correct choice of $\xi_1(0)$ and $\xi_2(0)$ must be found. These can be calculated, for example, using methods that rely on Newton iteration (Ascher and Petzold 1998). Results using the cost functionals $\mathcal{C}_A$ and $\mathcal{C}_B$ are presented in Fig. 5 with solid and dotted lines, respectively. The optimal stimuli, u^*, from each cost functional look qualitatively similar with those for $T_{\text{goal}}=22$ and 25 hours shown in the top-left and top-right panels of Fig. 5, respectively. When the optimal stimuli are applied to the full equations (59), the top-right panel compares the actual time at which $\theta=0$, denoted by T_{act} to the prescribed time T_{goal}. Similarly, the bottom-right panel shows the value of $\psi_1(T_{\text{goal}})$ after each control is applied to the full system. We find that the optimal stimuli obtained from $\mathcal{C}_A$ are more accurate than those obtained without correcting for changing phase dynamics. This is particularly apparent at for values of T_{goal} which are farther away from the natural period of $T=23.54$ hours. This happens because a larger change in the period requires more control effort, which takes the system farther from the limit cycle. Optimal stimuli obtained from $\mathcal{C}_A$ explicitly correct for changing phase and isostable dynamics, and ultimately provides an optimal control which satisfies the control objective better when applied to the full system.

4.3 Adaptation to external input in a neural model

Phase reduction is a useful tool in neuroscientific applications. In periodically spiking neurons, dynamics which give rise to neural action potentials can be understood in terms of the phase of oscillation (Ermentrout and Terman 2010) rather the complicated underlying state dynamics. Indeed, viewing neurons in terms of phase models has been particularly useful to understand the emergence of synchronization and complicated

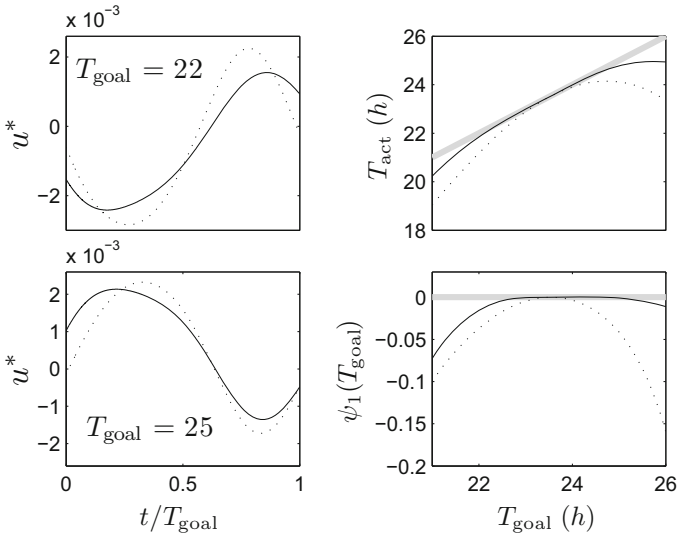

Fig. 5 Comparison of the optimal control resulting from using cost functionals C_A and C_B as *solid* and *dotted lines*, respectively. *Left panels* show the optimal waveform for two choices of T_{goal}. When applying the resulting optimal waveforms to the full system (59), the *top-right panel* compares the actual time at which $\theta = 0$, denoted by T_{act} to T_{goal}. The *grey line* represents perfect agreement between the goal and actual times at which $\theta = 0$. The *bottom-right panel* shows the value of $\psi_1(T_{\text{goal}})$ where the *horizontal grey line* represents the goal of $\psi_1(T_{\text{goal}}) = 0$

spiking patterns in large populations of neurons (Hoppensteadt and Izhikevich 1997; Tass et al. 2012; Azodi-Avval and Gharabaghi 2015; Wilson and Moehlis 2015).

One feature that standard phase models do not account for, however, is memory and adaptation effects (Cui et al. 2009; Ermentrout et al. 2001; Vreeswijk and Hansel 2001) whereby perturbations can have an effect on neurons on timescales that are slower than a single oscillation. The notion of a higher-order PRCs (Maran and Canavier 2008; Netoff and Schwemmer 2012), or functional PRCs (Cui et al. 2009) has been introduced to account for these effects in pulsed neural oscillators. While these effects are often necessary to consider in order to make accurate predictions about a neural phase locking behavior (Oprisan et al. 2004; Cui et al. 2009), such strategies cannot account for continuous perturbations and do not provide intuition about the underlying behavior responsible for the changing phase dynamics.

Here, we find that the reduction strategy proposed in this work can be used to understand and predict how slowly changing variables can affect the reduced phase dynamics leading to adaptation effects. We consider a three dimensional model for neural spiking behavior presented in Rubin and Terman (2004):

$$\begin{aligned} C\dot{V} &= -I_L(V) - I_{Na}(V,h) - I_K(V,h) \\ &\quad - I_T(V,r) + I_{SM} + I_{\text{ext}}(t), \\ \dot{h} &= (h_\infty(V) - h)/\tau_h(V), \\ \dot{r} &= (r_\infty(V) - r)/\tau_r(V). \end{aligned} \tag{64}$$

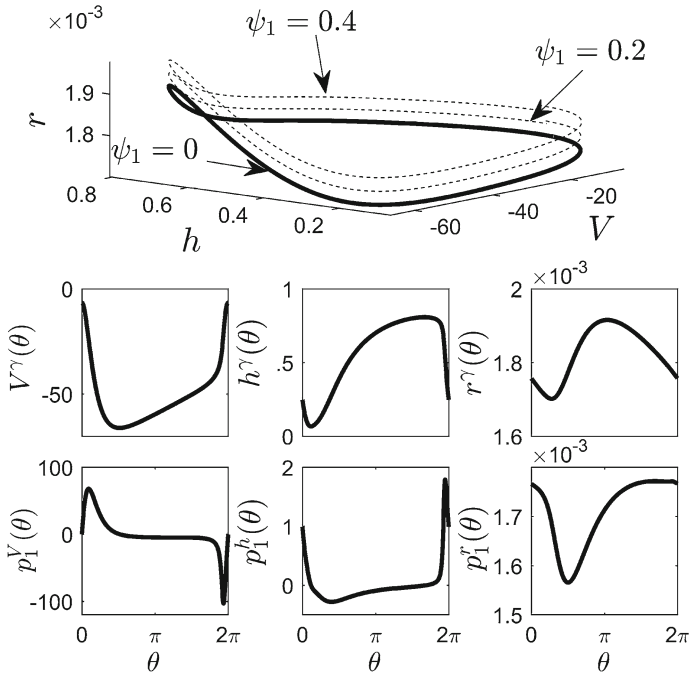

Fig. 6 The *top panel* shows the limit cycle solution x^γ as a *solid black line*. Positive isostable values correspond to the state increasing in the r-direction. The periodic orbit is represented as a function of θ in the *middle rows*, along with $p_1(\theta)$ in the *bottom rows*, which shows how the state changes as a function of θ and ψ_1

Here, V represents the transmembrane voltage, h and r are gating variables, $C = 1\ \mu\text{F/cm}^2$ is the membrane capacitance, $I_{\text{SM}} = 5\ \mu\text{A}/\mu\text{F}$ is the and $I_{\text{ext}}(t)$ is an external voltage perturbation. When $I_{\text{ext}}(t) = 0$, the system settles to a periodic limit cycle solution with natural period $T = 8.395$ ms. The limit cycle solution $x^\gamma(\theta) = [V^\gamma(\theta)\ h^\gamma(\theta)\ r^\gamma(\theta)]$ is shown in the second row of Fig. 6. In this model, we take, $\theta = 0$ to correspond to the moment that a neuron on the limit cycle spikes, taken to be the time it reaches its maximum transmembrane potential. A Poincaré return map is defined with respect to the $\theta = 0$ isochron and the values of the non-identity eigenvalues of its linear approximations are numerically determined to be $\lambda_1 = 0.828$ and $\lambda_2 = 0.045$. Similar to the previous example, we will approximate the $\psi_2 \approx 0$ (the isostable coordinate associated with λ_2) as perturbations in this direction decay rapidly on the time scale of a single neural spike. Based on the values of the parameters T and λ_1, $\omega = 0.748$ and $\kappa_1 = -0.023$. The periodic function $p_1(\theta) = [p_1^V(\theta)\ p_1^h(\theta)\ p_1^r(\theta)]^T$ (which is defined in (39) and how the state changes as ψ_1 changes) is calculated numerically using the approximation (37), and shown in the bottom row of Fig. 6. The top panel of Fig. 6 plots x^γ as a solid curve. Dotted curves show that increasing values of ψ_1 correspond to increasing values in the r-direction.

To illustrate the effect of memory in the neural model (64), consider the application of δ-function pulses at β ms intervals so that $I_{\text{ext}} = \alpha\delta(\text{mod}(t, \beta)$, with α being a

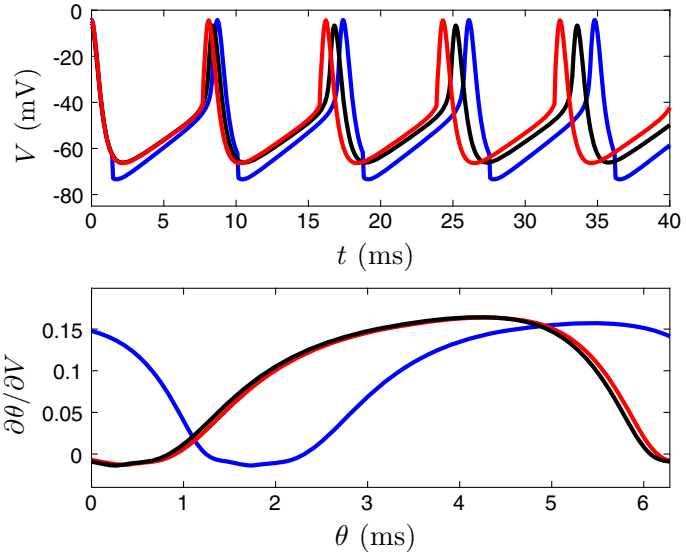

Fig. 7 In the *top panel*, *red* and *blue* voltage traces show the steady state behavior of (64) is entrained to 10 V (resp. -10 V) perturbations applied at 8.1 ms (resp. 8.7 ms) intervals. The *black trace*represents the limit cycle solution for reference. The *bottom panel* shows $\partial\theta/\partial V$ for each trajectory calculated using the direct method (Izhikevich 2007) with each *color* corresponding to the trace from the panel above. We interpret a shifting value of $\partial\theta/\partial V$ as adaptation, which is observed for negative perturbations, but not positive voltage perturbations (color figure online)

constant determining the magnitude of the perturbation. Here we will consider values of β close to the natural period so that the oscillator entrains in a 1:1 locking pattern to the pulsatile stimulus. The top panel of Fig. 7 shows examples a neuron entrained to a stimulus with $\alpha = 10$ mV, $\beta = 8.1$ ms, (resp. $\alpha = -10$ mV, $\beta = 8.7$ ms) with red (resp. blue) traces after allowing sufficient time for the transient behavior to die out. We also show an unperturbed neuron orbiting on the limit cycle as a black trace. The bottom panel gives the phase response for voltage perturbations evaluated numerically using the direct method (Izhikevich 2007) by applying a voltage perturbation ΔV at a known phase (i.e. isochron) and calculating $\partial\theta/\partial V \approx \Delta\theta/\Delta V$, with $\Delta\theta$ being the measured phase change due to the perturbation. Compared with the unperturbed system, after the system adapts to the negative perturbations, $\partial\theta/\partial V$ is shifted significantly to the right while the positive perturbations have little overall effect on adaptation.

Using the reduction (65), we can investigate the adaptation response of this neural system to these periodic, pulsatile inputs. The PRCs and IRCs, $Z(\theta) = [Z^V(\theta)\ Z^h(\theta)\ Z^r(\theta)]^T$ and $\mathcal{I}_1(\theta) = [\mathcal{I}_1^V(\theta)\ \mathcal{I}_1^h(\theta)\ \mathcal{I}_1^r(\theta)]^T$ are calculated using (16) and (31), respectively. In this example, we can only perturb the voltage variable, and $Z^V(\theta)$ and $\mathcal{I}_1^V(\theta)$ are shown in the left panel of Fig. 8. As in the previous example, $H_{\theta,x^\gamma(\theta)}$ and $H_{\psi_1,x^\gamma(\theta)}$ are calculated using (19) and (44), respectively. The partial derivatives with components in the V direction contribute to the reduction and are shown in the top-right panels. These functions are used in conjunction with $p_1(\theta)$ to calculate $C_1(\theta)$ and $D_1^1(\theta)$. The neural system (64) can be approximated by a reduction of the form (47):

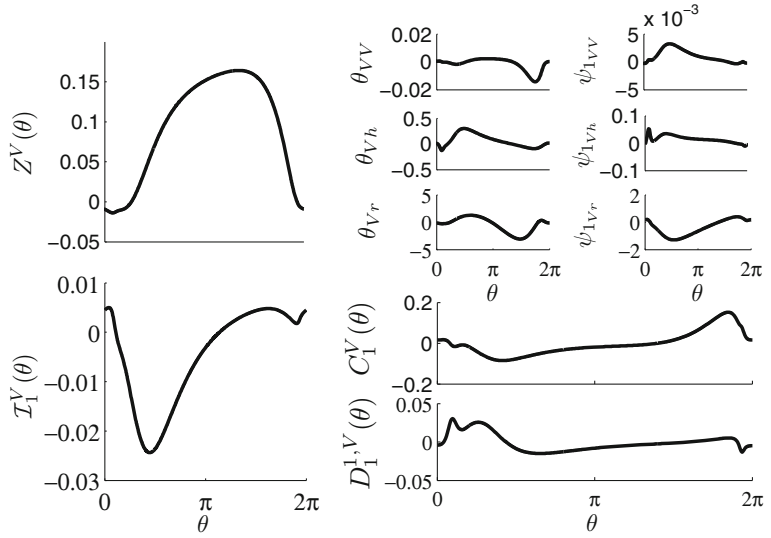

Fig. 8 Relevant parameters in the reduction of (64). *Left panels* show the PRC, $Z^V(\theta)$ and the IRC, $\mathcal{I}_1^V(\theta)$ for perturbations in the voltage direction. $C_1^V(\theta)$ and $D_1^{1,V}(\theta)$ provide corrections to the gradient of the phase and isostable coordinate, respectively, when the state is not on the limit cycle. These corrections are obtained using second order partial derivatives of the phase and isostable coordinates, calculated according to (19) and (44), respectively, and shown in the *top-right panels*

$$\begin{aligned}\dot{\theta} &= \omega + \left[Z^V(\theta) + \psi_1 C_1^V(\theta)\right] I_{\text{ext}}(t),\\ \dot{\psi}_1 &= \kappa_1 \psi_1 + \left[\mathcal{I}_1^V(\theta) + \psi_1 D_1^{1,V}(\theta)\right] I_{\text{ext}}(t),\end{aligned} \tag{65}$$

where, similar to the previous example, $C_1^V(\theta) = e_1^T H_{\theta,x^\gamma(\theta)} p_1(\theta)$, $D_1^{1,V}(\theta) = e_1 H_{\psi_1,x^\gamma(\theta)} p_1(\theta)$, and $e_1 = [1\ 0\ 0]^T$.

Letting $I_{\text{ext}}(t) = \alpha\delta(\text{mod}(t,\beta))$, where $\delta(t)$ is a delta function, β sets the rate of pacing, and α represents the magnitude of perturbations applied to the neuron. The dynamical behavior of the reduced system can then be understood in terms of a series of maps. By integrating (65) over the pulsing period, an initial condition $[\theta^-, \psi_1^-]$ corresponding to a time immediately proceeding a perturbation is mapped to

$$\begin{aligned}\theta^+ &= \text{mod}\big(\theta^- + \omega\beta + \alpha[Z^V(\theta^-) + \psi_1^- C_1^V(\theta^-)], 2\pi\big),\\ \psi_1^+ &= \big(\psi_1^- + \alpha[\mathcal{I}_1^V(\theta^-) + \psi_1^- D_1^{1,V}(\theta^-)]\big)\exp(\kappa_1\beta).\end{aligned} \tag{66}$$

Note that in (66), we assume that α is small enough so that the effect of delta function pulses can be well approximated with knowledge of gradient of the phase and isostable coordinates. We numerically calculate fixed points of (66), denoted by $[\theta^\infty, \psi_1^\infty]$, for various choices of α and β. In this example, we are interested ψ_1^∞ for these fixed points, as they determine the level of adaptation induced by the periodic perturbations. These values are shown in left panel of Fig. 9. For positive perturbations, ψ_1^∞ is relatively close to zero and $\partial\theta/\partial V$ does not change much compared to the

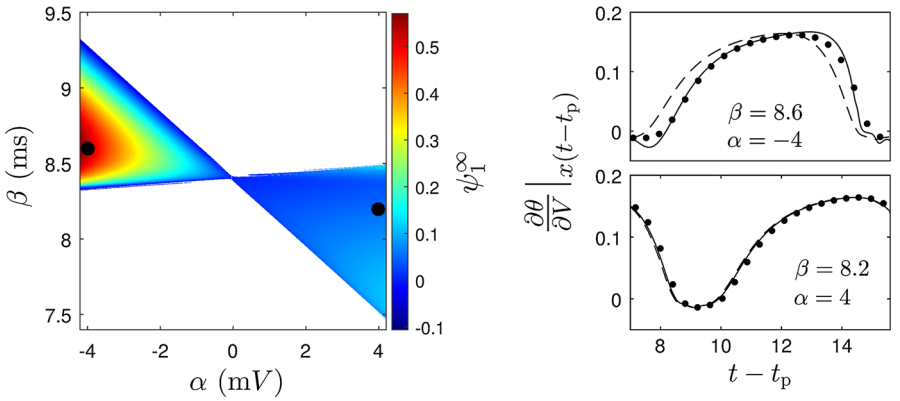

Fig. 9 The *left panel* gives the steady state value of ψ_1^+ of the map (66) indicating that significant adaptation is expected for negative perturbations while little adaptation is expected for positive perturbations. *White* indicates that the map has no fixed points those particular parameter values. *Black dots* in the *left panels* indicate parameter sets for which are investigated in the full model. *Right panels* illustrate the adaptation seen in the full model, when paced with the indicated parameters

unperturbed system. Negative perturbations, however, tend to result in much larger values of ψ_1^∞, particularly when they are close to the natural period. This effect can be seen by the change the value of $\partial\theta/\partial V$ for neurons with different pacing histories. For instance, in the top-right panel of Fig. 9 a single neuron is paced with a period $\beta = 8.6$ ms with pulses that perturb V by -4 mV. Once the neuron reaches steady state (i.e. the paced dynamics become periodic), the pacing is turned off. In these simulations, we denote the time of the final pulsatile perturbation by t_p. Individual dots represent direct measurements of $\partial\theta/\partial V$. The solid line represents the approximation $\partial\theta/\partial V \approx Z^V(\theta) + \psi_1 C_1^V(\theta)$ using initial conditions determined from the fixed point of (66). For comparison, the dashed line gives an approximation which does not account for adaptation, (i.e. $\partial\theta/\partial V \approx Z^V(\theta)$). The same test is implemented in the bottom-right panel of Fig. 9 with a period $\beta = 8.2$ ms for pulses which perturb V by 4 mV. As expected from the left panel of Fig. 9 even though the magnitude pulsing is the same, this parameter set does not produce much adaptation and both curves are nearly indistinguishable from each other. As ψ_1^∞ becomes larger, nonlinear terms begin to degrade accuracy of the prediction of $\partial\theta/\partial V$, however, the qualitative prediction of a shift to the right as ψ_1^∞ increases continues to hold.

5 Discussion and conclusion

Phase reduction continues to play in important role in the understanding of nonlinear limit cycle oscillations. Central to the utility of phase reduction is the assumption that an oscillator is on or close to its periodic orbit, limiting the magnitude of perturbations that can be applied without invalidating the assumptions of the reduction. In this work we have developed a closed set of reduced equations which correct for changes to the phase dynamics at locations further from the limit cycle. The reduction strategy presented here can be seen as a second order correction to the standard phase

reduction (9). While standard phase reduction techniques assume the state dynamics remain close to a one-dimensional subspace (the periodic orbit), the strategy presented here explicitly allows the state dynamics to exist on a higher dimensional subspace, necessitating the use of additional isostable coordinates in the overall reduction (47). The dynamics in some of these subspaces may decay rapidly allowing them to be effectively ignored, similar to the notion of an inertial manifold of a high dimensional system (Constantin et al. 1989; Foias et al. 1988; Jolly et al. 1990). In this case, even though a periodic orbit may be embedded in a high dimensional space, the reduced equations still represent a significant reduction in the complexity and dimensionality of the system if the exponential decay of some isostable coordinates is rapid.

The calculation of the second order partial derivatives of the phase and isostable coordinates are computationally intensive and may be a limiting factor for the application of this control strategy, especially in higher dimensional systems. Most notably, for the computation of PRCs and IRCs, the dimensionality of equations (16) and (31) scale with the number of state variables in the system while equations for finding the second partial derivatives, (19) and (44), scale with the square of the number of state variables. It may be of interest to develop strategies for the computation of these higher order partial derivatives using strategies with computational complexity which does not grow quadratically as the number of state variables increases. One such avenue of exploration may be to use the properties of the Koopman operator (Budišić et al. 2012); previous authors have noted that isostable coordinates can be defined as level sets of certain eigenfunctions of the Koopman operator (Mauroy et al. 2013; Shirasaka et al. 2017). Leveraging this property could lead to more efficient algorithms for computing isostable coordinates of large systems, particularly at locations far from the limit cycle.

While the reduction strategy presented here allows for a better understanding of phase reduced oscillators which have been perturbed from their nominal limit cycles, they still must remain reasonably close to their limit cycles to ensure accuracy of the reduction (47). While the accuracy may degrade due to higher order effects which are not explicitly accounted for by the approximation, it will still outperform the standard phase reduction (2) in most applications. In future work, it may be of interest to extend the reduction to include third order or higher corrections to the dynamics in (12).

The biologically inspired applications presented in this work illustrate some of the advantages of using the reduction (47) over a standard phase reduction (9). In a simple model of a circadian oscillator (59) an optimal control problem solved using the corrected phase reduction provides control signals which are much more effective than when using the uncorrected equations. Such a result is perhaps not surprising as the corrected phase reduced dynamics provide a better representation of the unreduced system. As perturbations become stronger, the corrected equations still suffer from similar limitations as the uncorrected phase equations, however, they will still give a better qualitative description.

This reduction strategy can also explicitly account for adaptation and memory effects that occur in a model based on the history of external perturbations applied to a model. This point is illustrated in a model of neural spiking, where we find that adaptation is a function of both the timing and magnitude of perturbations given in the model. When comparing the results presented here to other work on neural adaptation

it is important to note the definition of phase. Here, we define phase with respect to the infinite time convergence to the periodic orbit using isochrons (6), while others (Maran and Canavier 2008; Cui et al. 2009; Oprisan et al. 2004) define it with respect to the timing of the next spike with respect to the baseline firing rate. Both definitions have benefits and drawbacks, and it may be interesting to develop strategies to transform the reduction (65) from one definition of phase to the other. Neurons are not the only biological system which can adapt to external perturbations. For instance, the dynamics of excitable cardiomyocytes are strongly dependent on their pacing history (Tolkacheva et al. 2003; Cherry and Fenton 2004; Rosen and Cohen 2006). The present strategy might be able to be useful in the study of cardiological applications and where transient perturbations can have long lasting effects on system.

Acknowledgements Support for this work by National Science Foundation Grant NSF-1602841 is gratefully acknowledged.

References

Ascher UM, Petzold LR (1998) Computer methods for ordinary differential equations and differential-algebraic equations, vol 61. SIAM, Philadelphia

Azodi-Avval R, Gharabaghi A (2015) Phase-dependent modulation as a novel approach for therapeutic brain stimulation. Front Comput Neurosci 9:26

Bagheri N, Stelling J, Doyle FJ III (2008) Circadian phase resetting via single and multiple control targets. PLoS Comput Biol 4(7):e1000104

Brown E, Moehlis J, Holmes P (2004) On the phase reduction and response dynamics of neural oscillator populations. Neural Comput 16(4):673–715

Budišić M, Mohr R, Mezić I (2012) Applied Koopmanism. Chaos: an interdisciplinary. J Nonlinear Sci 22(4):047510

Castejón O, Guillamon A, Huguet G (2013) Phase-amplitude response functions for transient-state stimuli. J Math Neurosci 3:13

Cherry EM, Fenton FH (2004) Suppression of alternans and conduction blocks despite steep APD restitution: electrotonic, memory, and conduction velocity restitution effects. Am J Physiol Heart Circ Physiol 55(6):H2332–H2341

Constantin P, Foias C, Nicolaenko B, Temam R (1989) Integral manifolds and inertial manifolds for dissipative partial differential equations, vol 70. Springer, New York

Crowley SJ, Acebo C, Carskadon MA (2007) Sleep, circadian rhythms, and delayed phase in adolescence. Sleep Med 8(6):602–612

Cui J, Canavier CC, Butera RJ (2009) Functional phase response curves: a method for understanding synchronization of adapting neurons. J Neurophysiol 102(1):387–398

Dean DA, Forger DB, Klerman EB (2009) Taking the lag out of jet lag through model-based schedule design. PLoS Comput Biol 5(6):e1000418

Detrixhe M, Doubeck M, Moehlis J, Gibou F (2016) A fast Eulerian approach for computation of global isochrons in high dimensions. SIAM J Appl Dyn Syst 15(3):1501–1527

Ermentrout B, Pascal M, Gutkin B (2001) The effects of spike frequency adaptation and negative feedback on the synchronization of neural oscillators. Neural Comput 13(6):1285–1310

Ermentrout GB (2002) Simulating, analyzing and animating dynamical systems: a guide to XPPAUT for researchers and students. SIAM, Philadelphia

Ermentrout GB, Kopell N (1991) Multiple pulse interactions and averaging in systems of coupled neural oscillators. J Math Biol 29(3):195–217

Ermentrout GB, Terman DH (2010) Mathematical foundations of neuroscience, vol 35. Springer, New York

Foias C, Sell GR, Temam R (1988) Inertial manifolds for nonlinear evolutionary equations. J Differ Equ 73(2):309–353

Gonze D, Bernard S, Waltermann C, Kramer A, Herzel H (2005) Spontaneous synchronization of coupled circadian oscillators. Biophys J 89(1):120–129

Govaerts W, Sautois B (2006) Computation of the phase response curve: a direct numerical approach. Neural Comput 18(4):817–847
Grimshaw R (1993) Nonlinear ordinary differential equations, vol 2. CRC Press, Baca Raton
Guckenheimer J (1975) Isochrons and phaseless sets. J Math Biol 1(3):259–273
Guckenheimer J, Holmes P (1983) Nonlinear oscillations, dynamical systems, and bifurcations of vector fields, vol 42. Springer, New York
Guillamon A, Huguet G (2009) A computational and geometric approach to phase resetting curves and surfaces. SIAM J Appl Dyn Syst 8(3):1005–1042
Hoppensteadt FC, Izhikevich EM (1997) Weakly connected neural networks. Springer, New York
Huguet G, de la Llave R (2013) Computation of limit cycles and their isochrons: fast algorithms and their convergence. SIAM J Appl Dyn Syst 12(4):1763–1802
Ichinose N, Aihara K, Judd K (1998) Extending the concept of isochrons from oscillatory to excitable systems for modeling an excitable neuron. Int J Bifurc Chaos 8(12):2375–2385
Izhikevich EM (2007) Dynamical systems in neuroscience: the geometry of excitability and bursting. MIT Press, London
Jolly MS, Kevrekidis IG, Titi ES (1990) Approximate inertial manifolds for the Kuramoto–Sivashinsky equation: analysis and computations. Phys D Nonlinear Phenom 44(1):38–60
Kirk D (1998) Optimal control theory. Dover Publications, New York
Klausmeier CA (2008) Floquet theory: a useful tool for understanding nonequilibrium dynamics. Theor Ecol 1(3):153–161
Kuramoto Y (1984) Chemical oscillations, waves, and turbulence. Springer, Berlin
Kuramoto Y (1997) Phase-and center-manifold reductions for large populations of coupled oscillators with application to non-locally coupled systems. Int J Bifurc Chaos 7(04):789–805
Kurebayashi W, Shirasaka S, Nakao H (2013) Phase reduction method for strongly perturbed limit cycle oscillators. Phys Rev Lett 111(21):214101
Maran SK, Canavier CC (2008) Using phase resetting to predict 1:1 and 2:2 locking in two neuron networks in which firing order is not always preserved. J Comput Neurosci 24(1):37–55
Mauroy A, Mezić I, Moehlis J (2013) Isostables, isochrons, and Koopman spectrum for the action-angle representation of stable fixed point dynamics. Phys D Nonlinear Phenom 261:19–30
Nabi A, Mirzadeh M, Gibou F, Moehlis J (2013) Minimum energy desynchronizing control for coupled neurons. J Comput Neurosci 34:259–271
Netoff T, Schwemmer MA, Lewis TJ (2012) Experimentally estimating phase response curves of neurons: theoretical and practical issues. In: Phase response curves in neuroscience. Springer, pp 95–129
Oprisan SA, Prinz AA, Canavier CC (2004) Phase resetting and phase locking in hybrid circuits of one model and one biological neuron. Biophys J 87(4):2283–2298
Osinga HM, Moehlis J (2010) Continuation-based computation of global isochrons. SIAM J Appl Dyn Syst 9(4):1201–1228
Park Y, Ermentrout B (2016) Weakly coupled oscillators in a slowly varying world. J Comput Neurosci 40(3):269–281
Pyragas K, Novičenko V (2015) Phase reduction of a limit cycle oscillator perturbed by a strong amplitude-modulated high-frequency force. Phys Rev E 92(1):012910
Rabinovitch A, Thieberger R, Friedman M (1994) Forced Bonhoeffer-van der Pol oscillator in its excited mode. Phys Rev E 50(2):1572
Roberts AJ (1989) Appropriate initial conditions for asymptotic descriptions of the long term evolution of dynamical systems. The Journal of the Australian Mathematical Society. Series B. Appl Math 31(01):48–75
Rosen MR, Cohen IS (2006) Cardiac memory.. new insights into molecular mechanisms. J Physiol 570(2):209–218
Rubin J, Terman D (2004) High frequency stimulation of the subthalamic nucleus eliminates pathological thalamic rhythmicity in a computational model. J Comput Neurosci 16:211–235
Serkh K, Forger DB (2014) Optimal schedules of light exposure for rapidly correcting circadian misalignment. PLoS Comput Biol 10(4):e1003523
Shirasaka S, Kurebayashi W, Nakao H (2017) Phase-amplitude reduction of transient dynamics far from attractors for limit-cycling systems. Chaos: An Interdisciplinary. J Nonlinear Sci 27(2):023119
Strogatz SH (1994) Nonlinear dynamics and chaos: with applications to physics, biology, chemistry, and engineering. Addison-Wesley, Boston

Tass PA, Qin L, Hauptmann C, Dovero S, Bezard E, Boraud T, Meissner WG (2012) Coordinated reset has sustained aftereffects in parkinsonian monkeys. Ann Neurol 72(5):816–820

Tolkacheva EG, Schaeffer DG, Gauthier DJ, Krassowska W (2003) Condition for alternans and stability of the 1:1 response pattern in a model of paced cardiac dynamics. Phys Rev E 67(3):031904

van Vreeswijk C, Hansel D (2001) Patterns of synchrony in neural networks with spike adaptation. Neural Comput 13(5):959–992

Wedgwood KCA, Lin KK, Thul R, Coombes S (2013) Phase-amplitude descriptions of neural oscillator models. J Math Neurosci 3(1):2

Wilson D, Moehlis J (2014) An energy-optimal approach for entrainment of uncertain circadian oscillators. Biophys J 107(7):1744–1755

Wilson D, Moehlis J (2015) Clustered desynchronization from high-frequency deep brain stimulation. PLoS Comput Biol 11(12):e1004673

Wilson D, Moehlis J (2016) Isostable reduction of periodic orbits. Phys Rev E 94(5):052213

Winfree A (2001) The geometry of biological time, 2nd edn. Springer, New York

Xu Y, Padiath QS, Shapiro RE, Jones CR, Wu SC, Saigoh N, Saigoh K, Ptáček LJ, Fu YH (2005) Functional consequences of a CKIδ mutation causing familial advanced sleep phase syndrome. Nature 434(7033):640–644